International Journal of Structural Stability and Dynamics
Vol. 20, No. 10 (2020) 2042016 (26 pages)

DOI: 10.1142/S021945542042016X

World Scientific
www.worldscientific.com

# Comparative Modal Analysis of Monopile and Jacket Supported Offshore Wind Turbines including Soil-Structure Interaction

A. Abdullahi*, Y. Wang*,†,‡ and S. Bhattacharya*

*Department of Civil and Environmental Engineering
University of Surrey Guildford
Surrey GU2 7XH, UK

†School of Civil and Environmental Engineering
Harbin Institute of Technology (Shenzhen)
Shenzhen 518055, P. R. China
‡ying.wang@surrey.ac.uk;yingwang@hit.edu.cn

Received 1 October 2019
Accepted 26 March 2020
Published 18 September 2020

Offshore wind turbines (OWTs) have emerged as a reliable source of renewable energy, witnessing massive deployment across the world. While there is a wide range of support foundations for these structures, the monopile and jacket are most utilized so far; their deployment is largely informed by water depths and turbine ratings. However, the recommended water depth ranges are often violated, leading to cross-deployment of the two foundation types. This study first investigates the dynamic implication of this practice to incorporate the findings into future analysis and design of these structures. Detailed finite element (FE) models of Monopile and Jacket supported OWTs are developed in the commercial software, ANSYS. Nonlinear soil springs are used to simulate the soil-structure interactions (SSI) and the group effects of the jacket piles are considered by using the relevant modification factors. Modal analyzes of the fixed and flexible-base cases are carried out, and natural frequencies are chosen as the comparison parameters throughout the study. Second, this study constructs a few-parameters SSI model for the two FE models developed above, which aims to use fewer variables in the FE model updating process without compromising its simulation quality. Maximum lateral soil resistance and soil depths are related using polynomial equations, this replaces the standard nonlinear soil spring model. The numerical results show that for the same turbine rating and total height, jacket supported OWTs generally have higher first-order natural frequencies than the monopile supported OWTs, while the reverse is true for the second-order vibration modes, for both fixed and flexible foundations. This contributes to future design considerations of OWTs. On the other hand, with only two parameters, the proposed SSI model has achieved the same accuracy as that using the standard model with seven parameters. It has the potential to become a new SSI model, especially for the identification of soil properties through the model updating process.

*Keywords*: Offshore wind turbines; monopile; jacket; water-depth; turbine rating; cross-deployment; nonlinear springs; few-parameters SSI model.

‡Corresponding author.

## 1. Introduction

Offshore wind turbines (OWTs) have become increasingly important to modern societies that strive to meet their future targets of achieving sustainable and environmentally friendly energy utilization. However, structural stability is a concern for OWTs due to the operational and external loads they must endure. To militate against failure, appropriate support foundations must be carefully selected for each OWT. Although there are several foundation types for OWTs, Monopile and Jacket are the most deployed, accounting for 81.7% and 6.9% of all the existing European OWTs, respectively.[1] Foundation choice is largely influenced by water depth and turbine rating.[2] It was recommended that monopiles support OWTs at shallow water depths (less than 30 m) while jackets support them at transitional water depths (between 30–60 m).[3] Additionally, Abdullahi and Wang[4] found that jacket foundations were overwhelmingly deployed for turbine rating of 5 MW and above while monopile foundations were deployed to support OWTs with ratings of 4 MW and under, in the existing wind farms. However, these recommendations have often been violated as there are recorded cases of cross-deployments of the two foundation types. A few cases of these have been shown by Oh *et al.*,[5] for example, JSOWT-Jeju Island (15 m water depth), JSOWT-Thornton bank (12–26 m), JSOWT-NordseeOst (22–26 m) and MSOWT-Gunfleet sand 3 (supporting a 6 MW turbine).

The practice of cross-deployment of these two foundation types at similar depths may result in different dynamic responses of the system due to their varying mass/stiffness distributions, load transfer-mechanism, as well as interaction with the surrounding soil. It is important to investigate the varying dynamic responses of both OWTs for the understanding of their long-term performance. This is necessitated by the following consequences which could impact the safe and efficient operation of OWTs. First, for the same total height and turbine rating, OWTs supported on the two foundation types would have the same excitation frequencies of $1P$ (rotor frequency) and $3P$ (blade passing frequency), but different fundamental frequencies which are the most critical frequencies of OWTs. During the design process and operation stage, the fundamental frequencies of OWTs must be away from $1P$ (0.12–0.2 Hz) and $3P$ (0.35–0.6 Hz)[6] to preclude resonance.

Second, OWTs supported on the two foundation types would interact differently with the soil and would impact the natural frequency of the system differently as have been variously reported. References 7–9 investigated monopile-soil-interaction, while Jalbi and Bhattacharya[10] and Alati *et al.*[11] investigated jacket-soil interaction. To accurately account for the stiffness of the supporting soil and the dynamic properties of JSOWTs, all group effects, including modified $p$–$y$ and $t$–$z$ curves, should be included. However, the existing studies did not consider these effects. Finally, monopile and jackets have different serviceability limit criteria, e.g. a maximum rotation of 0.5°, Bisoi and Haldar[12] and 0.25°, Zhang *et al.*[13] are allowed at their sea beds, respectively. Therefore, it is critically important to investigate and

compare the modal characteristics of OWTs resulting from each foundation case as this is necessary for the accurate design of these structures.

Concerning the safe operation of OWTs, structural health monitoring (SHM) systems have been used, aiming to assess the health state of these facilities in real-time. As mentioned above, resonance preclusion is an important aspect of safe-guarding OWTs. Weijtjens *et al.*[14] conducted a study of the foundation monitoring of a full-scale operational OWT supported on a monopile foundation using the resonance frequencies of the system. An overall increase in the stiffness of the system was observed, which was attributed to the change in soil properties. Similarly, Xu *et al.*[15] recently carried out support condition monitoring and identification of an OWT model in the laboratory using experimental modal testing and finite element (FE) model updating methods. Vibrations experienced by the structure was found to have a minimal effect on the stress levels in the tower, thereby limiting the occurrence of local damage along its length. In contrast, changes in stress levels occurred on the pile inserted in the soil, this is consistent with the results of Refs. 8, 16 and 17. Based on these findings, changes in natural frequency of operational OWTs are attributed more to soil stiffness alterations rather than an occurrence of local tower damage. Model updating has proven a very useful tool in monitoring the health state of structures.[18,19] However, the deployment of this methodology is often hampered by a limit on the number of updating parameters that an algorithm can accommodate. Although the simplified methods (three and four spring models) give sufficiently accurate predictions of natural frequencies of OWTs,[20,21] they are most suitable for simple ground profiles and for predicting only the first natural frequency. For the more accurate simulation of a real OWT, e.g. with layered soils, distributed nonlinear spring models are often employed,[11,22,43] which normally contains more parameters that need to be updated.

To bridge the identified gaps in the current literature, this paper aims to

(1) Develop and validate the detailed FE models of monopile and jacket supported OWTs including SSI and use them to conduct comparative modal analyzes of MSOWTs and JSOWTs, to determine the dynamic implication of cross-deployment of these foundations.
(2) Develop a procedure that attempts to minimize the complications associated with the FE model updating of OWT-SSI systems by reducing the updating parameters.

Comparative modal analysis of MSOWT and JSOWT in water and a sandy deposit was conducted in this study to investigate the effect of cross-deployment of the two foundation types. First, detailed FE models of both structures, including SSI, were developed. Nonlinear soil springs, including group effects (in the case of jacket piles), were used to simulate soil resistance to loads from the OWT-foundation systems. The developed numerical models were verified by comparing their natural frequencies to those of similar structures in the literature.[11,23] Second,

few-parameters SSI models for both MSOWT and JSOWT were developed using polynomial equations. The results of their modal analyzes were compared with those from the existing SSI models.

## 2. Numerical Modeling

### 2.1. *Wind turbine prototype*

The NREL 5 MW wind turbine described in Ref. 23 is adopted in this study due to the easy accessibility of its properties, as well as its wide use in previous research which allows for comparison/validation of the models and analysis results.[23,24] This structure is a variable speed, collective pitch horizontal axis wind turbine, made up of an assembly of three blades, tower, nacelle and hub. The blades are connected to the hub, which is in turn, connected to the nacelle, forming the rotor-nacelle-assembly (RNA) supported on top of the tower. The tower is 87.6 m high tapered hollow cylindrical steel section with external diameters of 3.87 m and 6 m at the top and bottom, respectively. Its thickness increases linearly from 19 mm at the top to 27 mm at the bottom. The blades of the wind turbine are pre-twisted and made of eight airfoils and three circles, with different chord lengths. The corresponding airfoils are separated by unique distances, collectively amounting to 61.5 m (representing the total length of each blade). The hub diameter is 3 m. Table 1 shows the main properties of the wind turbine.

#### 2.1.1. *Monopile model*

The monopile model adopted in this study is a constant diameter hollow cylindrical steel section with a total length of 83.15 m and a constant wall thickness of 60 mm. Of its length, 18.15 m is above mean sea level, 30 m is in seawater and 35 m is embedded in the supporting soil. The detailed information of this model can be found in Fig. 1(a).

Table 1. Properties of NREL 5 MW wind turbine.[23]

| | | |
|---|---|---|
| Description | Turbine rating | 5 MW |
| | Rotor orientation | Upwind |
| | Rotor configuration | 3 blades |
| Tower | Height above MSL | 87.6 m |
| | Integrated mass | 3,47,460 kg |
| Blade | Rotor diameter | 126 m |
| | Length | 61.5 m |
| | Integrated mass | 17,740 kg |
| Hub | Height | 90 m |
| | Diameter | 3 m |
| | Mass | 56,780 kg |
| Nacelle | Mass | 2,40,000 kg |

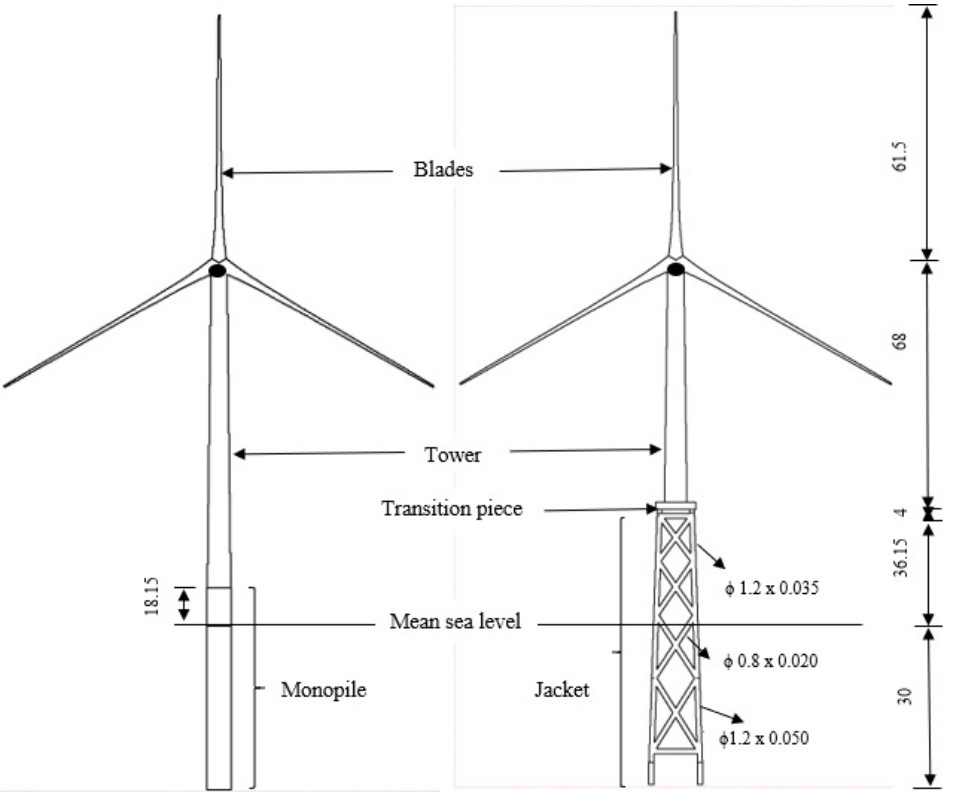


(a) MSOWT model (m) (b) JSOWTmodel (m)

Fig. 1. Front view of OWT models.

### 2.1.2. *Jacket model*

The jacket model adopted in this study is based on the IEA Wind Annex 30 OC4, Vorpahl and Kaufer,[25] which is a 70.15 m long tapered rectangular section, including the transition piece (a reinforced block of concrete with a 666 t mass). Cylindrical steel pipes constituting four levels of X-braces, four side-legs and one level of mud-braces, make up this support structure; the bottom and top widths are 12 m and 8 m, respectively. Four hollow cylindrical steel piles, (each with external diameters, thickness, penetration, and a center-to-center spacing in the direction of loading of 2.082 m, 0.06 m, and 35 m, 12 m, respectively,) support the jacket and tower-RNA, thus, forming the JSOWT assembly.

To make the JSOWT comparable to the MSOWT, the heights above the mudline are made the same. The height of the JSOWT tower is reduced by 22 m from the base. The transition piece together with the upper jacket-support has a total height of 40.15 m above mean sea level. The lower jacket length is 30 m in seawater, and the supporting piles penetrate the soil to a depth of 35 m, both of which are the same as those of MSOWT. The detailed model is shown in Fig. 1(b).

### 2.2. *Finite element model*

Based on the prototype, a detailed 3D model of the NREL 5 MW wind turbine is initially developed using the computer-aided design program, Autodesk Inventor, which is then converted to an FE model using the commercial software, ANSYS.

The tower and blades are modeled by the shell element (SHELL181 in ANSYS), while the masses of the hub and nacelle are incorporated into the FE model by lumping them on top of the tower. To capture the effect(s) of the blade geometry on the dynamic response(s) of the OWTs, the blade profile is explicitly modeled. Element sizes of 1 m and 0.5 m are, respectively, chosen in the axial and circumferential directions of the tower and blades, as suggested by Zuo *et al.*,[26] and confirmed by the convergence test in this study (Sec. 3.1). This modeling achieves a good balance of computational time and accuracy.

The monopile lengths above and beneath the mudline are modeled by the shell (SHELL181 in ANSYS) and beam elements (BEAM188 in ANSYS), respectively. The latter is for the convenient consideration of SSI. The same element size as the tower is chosen for the monopile (i.e. 1 m and 0.5 m for the axial and circumferential directions, respectively). To guarantee the same deformation between the monopile and tower, the cross-section of the former is tied to the base of the latter (Ref. 26).

The jacket support is modeled by the shell element (SHELL181 in ANSYS), while its supporting piles are modeled by the beam element (BEAM188 in ANSYS), with the adjoining cross-sections, also tied to each other. The same element size of 1 m and 0.5 m are, respectively, chosen for the axial and circumferential directions of the jacket members.

The wind turbine blades are made of polyester material, with a density of 1850 kg/m$^3$. The tower and monopile/jacket are made of steel, with densities of 8500 kg/m$^3$ and 7850 kg/m$^3$, respectively. Jonkman *et al.*[23] estimated that the density of monopile/jacket in sea water is 8880 kg/m$^3$, to account for additional masses of paints, bolts, ladders, welds, as well as water-monopile/jacket interaction resulting from the vibrating monopile/jacket which excites acceleration to the surrounding seawater (Zuo *et al.*,[24]). Table 2 shows the material properties of the different parts of both OWTs.

To ensure that the developed FE models demonstrate the same dynamic behaviors as the prototype OWTs, the FE modeling is carried out in stages, as

Table 2. Material properties of MSOWT and JSOWT (Refs. 23–25).

| Component | Material | Density (kg/m$^3$) | Young's modulus (GPa) | Poisson's ratio | Yield strength (MPa) | Plastic strain |
|---|---|---|---|---|---|---|
| Blade | Polyester | 1850 | 38 | 0.3 | 700 | 0.02 |
| Tower | Steel | 8500 | 210 | 0.3 | 235 | 0.01 |
| Monopile and Jacket in water | Steel | 8880 | 210 | 0.3 | 235 | 0.01 |
| Monopile and Jacket above mudline | Steel | 7850 | 210 | 0.3 | 235 | 0.01 |

benchmarking operations. This approach ensures that each benchmarked part of the FE model is developed to a sufficient level of accuracy while preparing the ground to embark on the next phase of modeling. In the first step, the fixed base wind turbine (without SSI consideration) is modeled and benchmarked. In the second

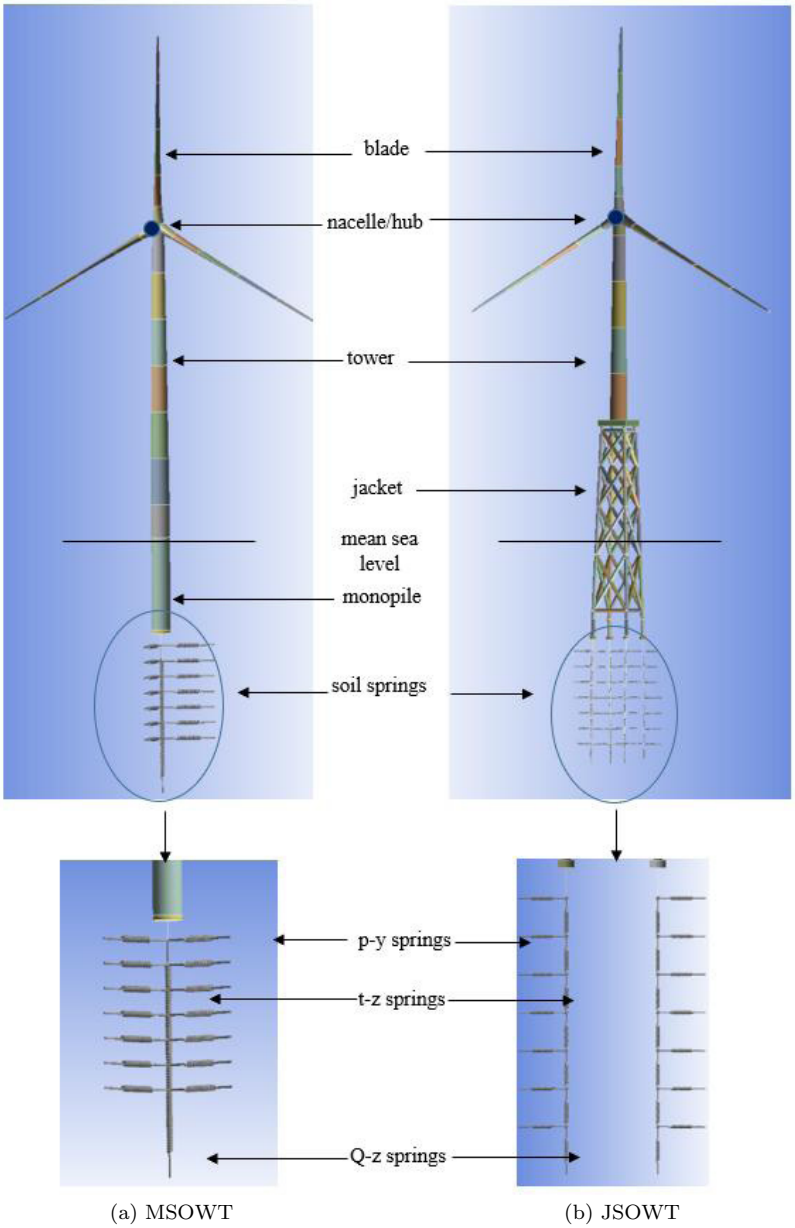


(a) MSOWT (b) JSOWT

Fig. 2. FE models of OWTs including SSI.

step, the monopile and jacket foundations are attached to the initially benchmarked model, without SSI consideration. In the third and final step, the SSIs are modeled for both MSOWT and JSOWT. The described FE models are shown in Fig. 2.

### 2.3. *Soil-structure interaction*

As shown in the literature, the dynamic behaviors of OWTs are significantly affected by the interaction(s) between the foundations and the surrounding soil. Jalbi *et al.*[27] broadly categorized the methods used to simulate these interactions into three groups, which include: the simplified, standard and advanced methods, as shown in Fig. 3. The distributed nonlinear spring model ($p$–$y$, $t$–$z$ and $Q$–$z$) used in del Campo *et al.*[28]; Harte and Basu[29] constitutes the standard method; the simplified methods include both the three-springs model (lateral, rotational and vertical springs, described in Ref. 30) and four-spring models (lateral, rotational, vertical and rotational-lateral coupled springs, as described in Refs. 8 and 21). The advanced method involves the use of FE analysis along with sophisticated soil models, e.g. (Ref. 31).

Due to the balance of both the accuracy and simplicity of the standard method, it is adopted in this research. Distributed nonlinear Winkler springs are used to simulate the interaction between the soil and pile-wind turbine system in the axial and lateral directions. As recommended in API,[32] $p$–$y$ springs account for lateral soil stiffness against foundation movement; $t$–$z$ springs account for axial skin friction against vertical foundation movement, and $Q$–$z$ springs account for soil end-bearing to pile tip. The spacing between successive sets of soil springs is chosen based on the aim of the study. For example, Bisoi and Haldar[12] modeled the springs with 1 m spacing, while Zuo *et al.*[24] chose 10 m spacing. In this study, the spacing is selected as 5 m. Figures 2(a) and 2(b) show the FE models of MSOWT and JSOWT with their

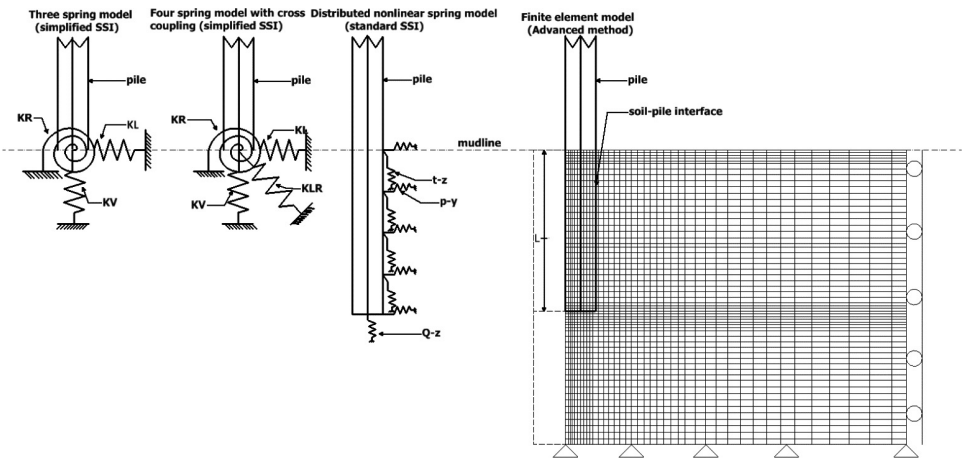


Fig. 3. Soil-structure interaction models of piles.

respective soil springs. Figures 3 and 4, respectively, show the different SSI modeling methods and detailed models of soil-pile interactions for MSOWT and JSOWT attached to soil springs in this study.

In this study, only dense sand is considered. As recommended in API,[1] the lateral soil resistance per unit length of the pile, $p$, (N/m) is related to its unit deflection, $y$, by the following expression:

$$p = A \cdot pl \cdot \frac{\tanh(k \cdot H)}{A \cdot pl} \cdot y, \tag{1}$$

where $A$ is a factor accounting for cyclic or static loading conditions:

$$A = 0.9 \quad \text{for cyclic loading;} \tag{2}$$

$$A = \left(3.0 - 0.8\frac{H}{D}\right) \geq 0.9 \quad \text{for static loading,} \tag{3}$$

where $k$ is the initial modulus of subgrade reaction (kN/m$^3$); $y$ is the lateral deflection (m), and $D$ is the average pile diameter (m). $pl$ is the ultimate unit lateral bearing capacity of the soil (N/m) at depth $H$ (m), which varies from shallow (pls) to deep

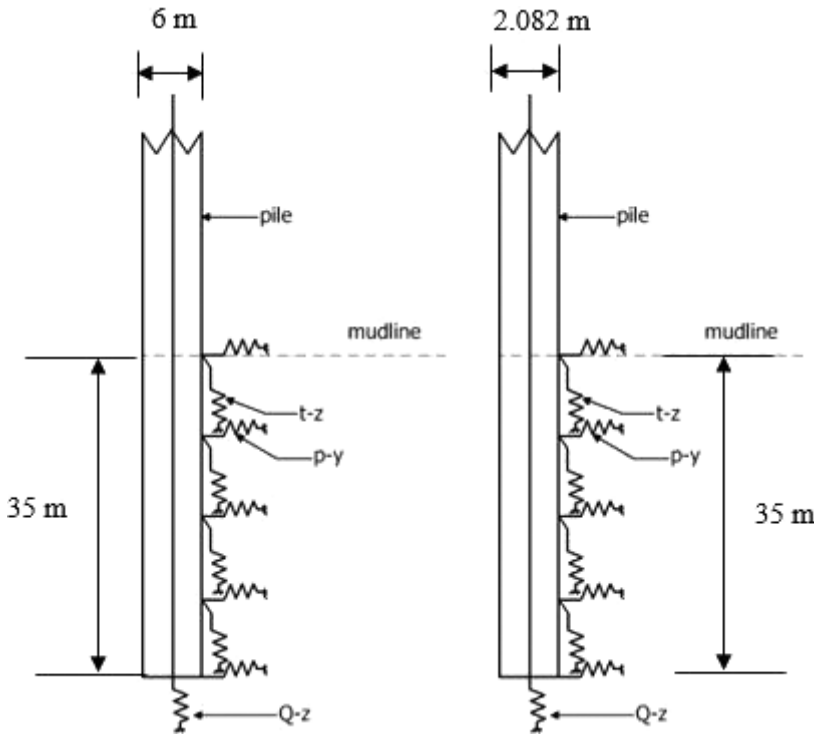


(a) MSOWT SSI (b) JSOWT SSI

Fig. 4. OWT soil-pile interaction models.

depths (pld). They can be estimated based on the following formulations as recommended in API[32]:

$$\text{pls} = (C_1.H + C_2.D)\gamma \cdot H, \tag{4}$$

$$\text{pld} = C_3 \cdot D \cdot \gamma \cdot H, \tag{5}$$

$$\text{pl} = \min(\text{pls}, \text{pld}), \tag{6}$$

where $\gamma$ is the effective soil weight (kN/m$^3$); $C_1, C_2$ and $C_3$ are coefficients determined as functions of the angle of internal friction, $\phi$ (degrees)

In this study, $C_1C_2$, $C_3$ and $k$ are, determined for Red Hill Silica sand with basic properties:

$$\gamma = \frac{16.8\,\text{kN}}{\text{m}^3}, \quad \phi = 36^\circ \quad \text{(Ref. 15)}.$$

To quantify the $t$–$z$ and $Q$–$z$ spring stiffnesses, $t$, $t_{\max}$, $Q$ and $Q_p$ need to be computed. Here, $t$ and $t_{\max}$ are the mobilized and maximum soil-pile adhesions (kPa), respectively, which are computed for dense sand according to API[32] as follows:

$$t = K \cdot \sigma \cdot \tan\delta \leq 95.7, \tag{7}$$

$$t_{\max} = K \cdot \sigma \cdot \tan\delta \cdot \pi \cdot D, \tag{8}$$

$$\delta = (\phi - 5), \tag{9}$$

where $K$ is the coefficient of lateral earth pressure, assumed as 0.8 for open-ended pipes under compression and tension loadings; $\sigma$ is the effective overburden pressure at the considered depth, and $\delta$ is the friction angle between the soil and pile wall, and $z$, is the axial pile deflection.

$Q$ and $Q_p$ are the mobilized and end-bearing capacities of the pile (kPa), respectively, which are given for dense sand by API[32] as

$$Q = \sigma \cdot N_q, \tag{10}$$

$$Q_p = \sigma \cdot N_q \cdot \pi \cdot \frac{D^2}{4}, \tag{11}$$

where $N_q$ is the dimensionless bearing capacity factor.

Substituting $t_{\max}, Q_p$ and $D$ into their respective tables in API,[32] the $t$ versus $z$ and $Q$ versus $z$ relationships are obtained.

#### 2.3.1. *Group effects of piles*

While the use of the $p$–$y$ method has proven reliable for evaluating the response of single piles under horizontal load, researchers, such as Shi *et al.*,[33] questioned its reliability in assessing the response of pile groups under similar loading, considering such factors as the shadowing effect of group piles (Refs. 34 and 35). A widely adopted method (Rollins *et al.*[36]) was proposed to account for group pile-soil interaction in jacket structures for pile spacing to diameter ratio, $(\frac{S}{D})$, of less than the

marginal value of 6.5. It modifies the single $p$–$y$ curves using a multiplier factor, $P_m$, as suggested by Ref. 37. The dynamic soil reaction of a group of piles, $p_g$, at a certain depth is given as

$$p_g = p_m p, \tag{12}$$

where $p$ is the lateral soil resistance per unit length of a single pile at the same depth; $p_m$ is a multiplier defined for each row depending on the pile diameter ($D$), piles spacing ($S$), and row position in the loading direction as shown in Fig. 5. $p_m$ can be calculated from the following equation (Shi *et al.*[33]):

$$\text{First row piles}: \ p_m = 0.26 \ln(S/D) + 0.5. \tag{13}$$

$$\text{Second-row piles}: \ p_m = 0.52 \ln(S/D). \tag{14}$$

$$\text{Third and higher row piles}: \ p_m = 0.6 \ln(S/D) + 0.25. \tag{15}$$

For the pile group in this study, $\frac{S}{D} = 5.764$, which is less than the group marginal value of 6.5 (Rollins *et al.*[36]), therefore, $p$–$y$ group effect is considered. Utilizing Eqs. (12) and (13), $p_m$, for the first and second rows of the pile group are 0.955 and 0.911, respectively. These values are thus multiplied by the $p$ values of single piles in the respective rows they occur.

For group piles deriving their load capacity from both side-adhesion and end-bearing, Chellis[38] recommended that only side-adhesion group effect should be taken into account, taking the end bearing efficiency as unity (Ref. 39). For sand, group pile shaft friction efficiency, $t_m$ is a multiplier mostly greater than 1, as shown by the tests conducted by Kezdi[40] and Cambefort[41] on large diameter piles in groups of four and nine, respectively. This is calculated as a function of pile spacing $S$ and diameter $D$. Based on the $S$ and $D$ values in this study, the $t_m$ values are calculated as 1.1 and 1.17, respectively. An average value of 1.14 is used as the $t_m$ value.

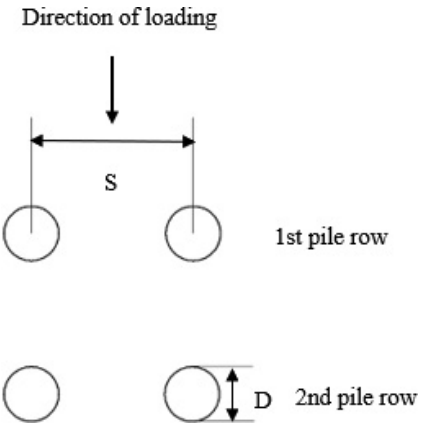


Fig. 5. The Layout of a group of four piles and their direction of loading.

### 2.3.2. *Development of few-parameters SSI model*

Based on the previous findings, e.g. Xu *et al.*[15] and Weijtjens *et al.*,[14] natural frequency changes in OWTs under long term vibrations, primarily result from soil stiffness changes around the foundation, rather than the occurrence of structural

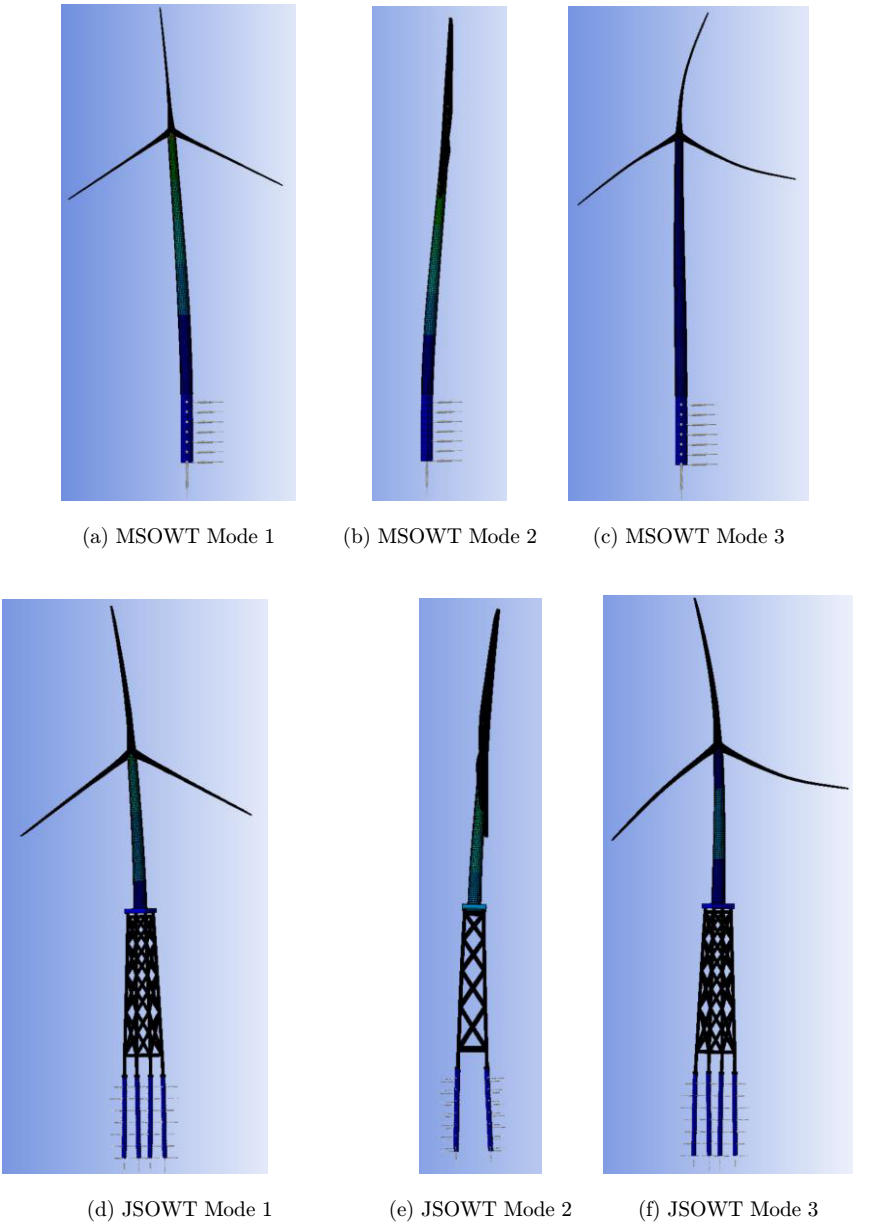

(a) MSOWT Mode 1 (b) MSOWT Mode 2 (c) MSOWT Mode 3

(d) JSOWT Mode 1 (e) JSOWT Mode 2 (f) JSOWT Mode 3

Fig. 6. First three Mode shapes of MSOWT and JSOWT.

failure on the superstructure. FE model updating method has shown success in the identification of unknown soil spring stiffness parameters (Xu *et al.*[15]). It is widely accepted that the model updating performance inevitably decreases with the increase in the number of updating parameters (Ref. 42). For model updating operations on the MSOWT and JSOWT FE models in this study, the SSI parameters in all the soil layers need updating, which may affect the updating performance negatively. Therefore, a few-parameters-SSI model method is proposed to reduce the number of updating parameters.

Because the lateral loads on OWTs from wind and waves far outweigh those from their self-weights, load capacities in the lateral direction (*p–y curves*) play the most significant role in stabilizing the foundations for the vibrations they experience, as will be shown in the next section. Therefore, *p–y curves* are utilized in the development of few-parameters SSI model. The maximum lateral resistance, $p_{\max}$, of the soil supporting the superstructures of the detailed OWT FE models, is chosen as the target parameter influencing the natural frequencies of the entire systems. For each considered depth, $H(m)$, along the pile lengths, $p_{\max}(N)$ occurring at maximum lateral displacement, $y_{\max}(m)$, is calculated; a plot of $p_{\max}$ against $H$ is then made, wherefrom, a curve describing the relationship between the two parameters emerges. A polynomial equation is proposed to fit the curve, representing the relationship between $p_{\max}$ and $H$. Since we assume that there is no displacement at the centreline of the bottom of the pile ($p_{\max} = 0$ when $H = 0$), the constant term is set as 0.

$$p_{\max} = \sum_{i=1}^{n} \propto_i H^i, \tag{16}$$

where $\propto_i$ represents constants (in this case, defined by soil properties and foundation form/geometry), while $n$ is the degree of the polynomial equation defining $p_{\max}$ and $H$ relationship. This single equation defines $p_{\max}$ for any depth along the length of the buried pile, thereby reducing an otherwise complex model to a few-parameters one.

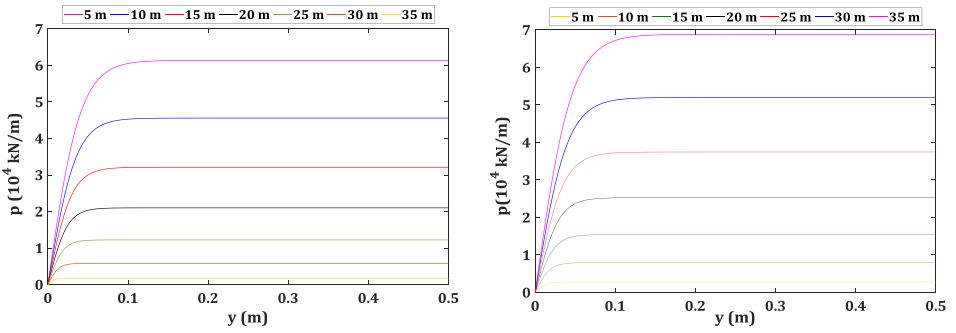


(a) *p–y* curve of JSOWT (b) *p–y* curve of MSOWT

Fig. 7. Nonlinear soil springs for MSOWT and JSOWT.

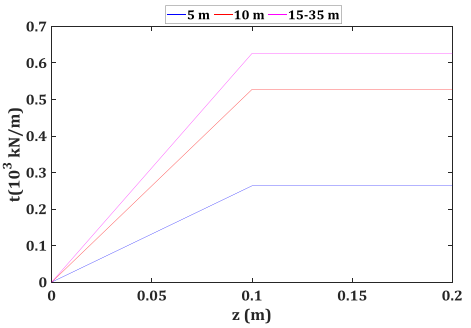


(c) $t$–$z$ curve for JSOWT

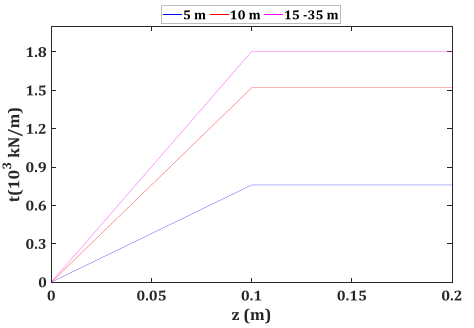


(d) $t$–$z$ curve for MSOWT

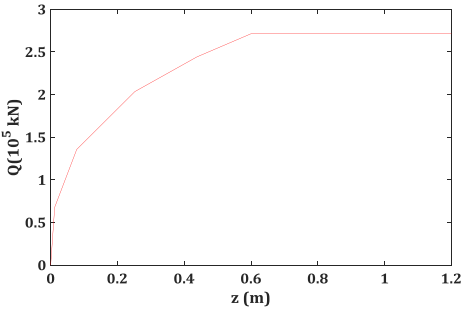


(e) $Q$–$z$ curve for JSOWT

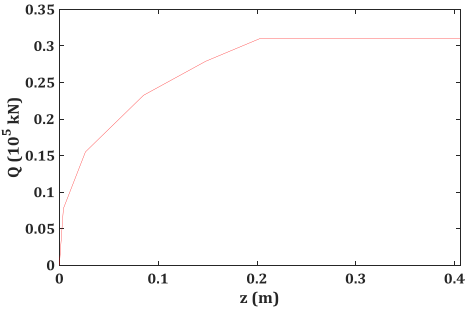


(f) $Q$–$z$ curve for MSOWT

Fig. 7. (*Continued*)

Relying on the fact that the $p$–$y$ soil springs for both foundation types exhibit elastic-plastic deformations as shown in Figs. 7(a) and 7(b), the formulation for estimating soil stiffness, $Q(N/m)$, as described in Augustesen *et al.*,[22] is used in this study. For any depth, the calculated $p_{\max}$ from Eq. (16), along with its corresponding $y_{\max}$ from the $p$–$y$ curve, are used to compute the soil stiffness as given in Eq. (17).

$$V_j = P_{\max j}/y_{\max j}. \tag{17}$$

## 3. Numerical Studies

### 3.1. *Verification of FE models*

The NREL 5 MW wind turbine is adopted as the superstructure for both the Monopile and Jacket foundations in this study. Due to the strong link between the accuracy of FE analysis and size of elements, a convergence test was carried out to obtain an optimum element size. The modal analysis of the developed FE model was performed in ANSYS with the tower base and blades in fixed and parked positions, respectively, where modal parameters (in this case, natural frequencies and mode

shapes) were obtained. The first fundamental natural frequency of the wind turbine is chosen as the convergence test feature. Element size pairs in the axial and circumferential directions of the tower and blades are selected as mesh cases for the scheme as shown in Table 3. Mesh cases are defined thus: 'case 2' corresponding to '2–1', for example, denotes element size of 2 m in the axial direction of the tower and blades, and 1 m in the circumferential direction of the tower and blade. Using these mesh cases, the first fundamental frequency of the wind turbine for the respective cases was obtained, as shown in Table 3. A satisfactory convergence was observed in mesh 'case 5', having element sizes of 1 m and 0.5 m in the axial and circumferential directions of the tower and blades, respectively. This element size was therefore adopted throughout the study.

To validate the superstructure of the developed wind turbine FE model (excluding foundation), modal analysis was performed in ANSYS. The first 12 natural frequencies and their associated vibration modes were compared to those in Jonkman *et al.*,[23] as shown in Table 4.

Respective natural frequencies were matched to their corresponding vibration modes by animating their deformation modes in ANSYS. Visualized examples of these are shown in Fig. 6. Based on the comparison results, good agreements are generally observed, especially for those related to the support structure, the average

Table 3. Mesh size cases for convergence studies.

| Test number. | Mesh case | Fundamental frequency (Hz) |
|---|---|---|
| 1. | 2–2 | 0.381 |
| 2. | 2–1 | 0.348 |
| 3. | 2–0.5 | 0.324 |
| 4. | 1–1 | 0.305 |
| 5. | 1–0.5 | 0.302 |
| 6. | 0.5–0.5 | 0.302 |

Table 4. Natural frequencies of fixed-base NREL 5 MW wind turbine in a parked condition.

| Mode | Description | Jonkman *et al.*[23] (Hz) | Present study (Hz) | Difference (%) |
|---|---|---|---|---|
| 1 | First support structure side-to-side | 0.312 | 0.302 | 3.3 |
| 2 | First support structure fore-aft | 0.324 | 0.313 | 3.4 |
| 3 | First blade flapwise yaw | 0.666 | 0.497 | 25.3 |
| 4 | First blade flapwise pitch | 0.668 | 0.574 | 14.1 |
| 5 | First blade collective flapwise | 0.699 | 0.720 | −3.0 |
| 6 | First blade edgewise pitch | 1.079 | 0.819 | 24.1 |
| 7 | First blade edgewise yaw | 1.090 | 0.953 | 12.5 |
| 8 | Second blade flapwise yaw | 1.934 | 1.589 | 17.8 |
| 9 | Second blade flapwise pitch | 1.922 | 1.820 | 5.3 |
| 10 | Second blade collective flap | 2.021 | 2.290 | −13.3 |
| 11 | Second support structure side-to-side | 2.936 | 3.327 | 9.2 |
| 12 | Second support structure fore-aft | 2.900 | 2.666 | 8.1 |

difference being 6% and thus, marking a successful initial benchmarking. Although the frequencies related to blades show slightly larger differences, the average being 12.84%. This is due to a lack of explicit information about the geometrical and material properties of the strengthening webs and nacelle. With such information, the differences are expected to be substantially reduced.

Following the benchmarking of the super structure model, fixed bases of the monopile and jacket foundations are introduced to the relevant lengths of the benchmarked FE model; modal analyzes were performed in ANSYS. For model validation, the first natural frequency of the fixed-base MSOWT model excluding the length in soil, as obtained from ANSYS, is compared to the analytically obtained natural frequency using the closed-form solution described in Arany *et al.*[5] 0.203 Hz and 0.21 Hz were obtained for the two respective cases; this difference amounts to 3.3%, which indicates a good agreement between both results, hence, validating the model.

Similarly, the fixed-base JSOWT FE model was validated by comparing its first 12 natural frequencies to those in Alati *et al.*,[11] as shown in Table 5. In general, good agreements are observed; the jacket-tower frequencies occurring in corresponding vibration modes show very close agreements, with an average difference of 1.8%, while the blade frequencies show slightly larger differences due to the absence of strengthening webs in the FE model, with an average difference of 8.69%. Furthermore, the first natural frequency from this study (in Table 5) is compared to that from a closed-form solution (Ref. 10). Respective values of 0.309 Hz and 0.303 Hz are obtained; this difference amounts to only 1.9%, indicating a good agreement between both results, thus, validating the FE model.

### 3.2. *Comparative modal analysis of fixed-base OWTs*

To investigate the influence of foundation type on the natural frequencies of OWTs supported on monopiles and jackets, modal analyzes were conducted on the

Table 5. Natural frequencies of fixed-base 5 MW NREL JSOWT in a parked condition.

| Mode | Description | (Alati *et al.*,[11]) (Hz) | Present study (Hz) | Difference (%) |
|---|---|---|---|---|
| 1 | First support structure side-to-side | 0.314 | 0.309 | 1.6 |
| 2 | First support structure fore-aft | 0.317 | 0.321 | −1.4 |
| 3 | First blade flapwise yaw | 0.640 | 0.554 | 13.4 |
| 4 | First blade flapwise pitch | 0.675 | 0.664 | 1.6 |
| 5 | First blade collective flapwise | 0.708 | 0.720 | −1.6 |
| 6 | First blade edgewise pitch | 1.080 | 0.864 | 20.0 |
| 7 | First blade edgewise yaw | 1.092 | 0.880 | 19.4 |
| 8 | Second blade flapwise yaw | 1.714 | 1.774 | −3.5 |
| 9 | Second blade flapwise pitch | 1.937 | 2.006 | −3.6 |
| 10 | Second blade collective flap | 2.003 | 2.480 | −23.8 |
| 11 | Second support structure side-to-side | 1.219 | 1.168 | 4.2 |
| 12 | Second support structure fore-aft | 1.241 | 1.241 | 0.0 |

validated fixed-base cases. The first 12 natural frequencies were obtained (shown in Table 6). It was observed that except for the second-order blade modes, significant differences occur between the vibration frequencies of OWTs supported on the two foundation types, even though they are designed to support equally rated turbines. Natural frequencies of the JSOWT were found to be higher than those supported on monopiles in the first-order support modes, while the reverse is true in the second-order support modes. In contrast, the blade modes remained relatively similar.

In this study, the fundamental frequencies of both structures are well clear of both $1P$ and $3P$ frequency ranges, and thus cross deployment does not lead to resonance in this case (fixed base). However, the first-order support modes of MSOWT and JSOWT show the largest natural frequency differences, i.e. 50.9% and 51.8%, respectively. These variations are a direct consequence of their different stiffness and mass properties as they occur in the fundamental frequency equation. The mass contribution to the natural frequency may not necessarily be the total mass, but is related to the density of the materials as well as the geometry of the structure, from which the 'effective mass', which directly relates to the natural frequency, is obtained (Ref. 21). Based on the formulations in Arany *et al.*[20] and Jalbi and Bhattacharya,[10] the effective masses of both MSOWT and JSOWT are computed as $537,722$ and $5,00,217\,\text{kg}$, respectively, while the computed stiffness are $7.5 \times 10^5\,\text{N/m}$ and $1.9 \times 10^6\,\text{N/m}$, respectively. Considering the different properties, it is obvious that the jacket provides a higher stiffness to the OWT than the monopile, with a difference of up to 153%. On the other hand, the effective masses of both structures are close, with the MSOWT slightly heavier (less than 7%) than the JSOWT. The stiffness-to-mass ratios of the MSOWT and the JSOWT are 1.4 and 3.8, respectively. The fundamental natural frequency differences are therefore attributed to the superior stiffness the jacket provides over the monopile in supporting the OWT superstructure. Therefore, when designing the OWTs, the foundation type/size should be carefully investigated for resonance preclusion.

Table 6. Natural frequencies and modes for fixed-base MSOWT and JSOWT.

| Mode | Description | MSOWT frequency (Hz) | JSOWT frequency (Hz) | Difference (%) |
|---|---|---|---|---|
| 1 | First support structure side-to-side | 0.203 | 0.309 | −51.8 |
| 2 | First support structure fore-aft | 0.207 | 0.313 | −50.9 |
| 3 | First blade flapwise yaw | 0.505 | 0.554 | −9.7 |
| 4 | First blade flapwise pitch | 0.619 | 0.664 | −7.3 |
| 5 | First blade collective flapwise | 0.724 | 0.720 | 0.7 |
| 6 | First blade edgewise pitch | 0.846 | 0.864 | −2.1 |
| 7 | First blade edgewise yaw | 0.893 | 0.880 | 1.4 |
| 8 | Second support structure side-to-side | 1.480 | 1.168 | 21.1 |
| 9 | Second support structure fore-aft | 1.524 | 1.241 | 18.6 |
| 10 | Second blade flapwise yaw | 2.155 | 1.774 | 17.7 |
| 11 | Second blade collective flapwise | 2.490 | 2.480 | 0.4 |
| 12 | Second blade flapwise pitch | 2.030 | 2.029 | 0.5 |

### 3.3. *Comparative modal analysis of OWTs including SSI*

To investigate the different effects of SSI on the natural frequencies of OWTs supported on monopile and jacket foundations, a common buried pile length in soil, is defined (here, 35 m). Properties of each pile and a homogenous sandy soil (Red Hill silica sand) were used to calculate distributed $p$–$y$, $t$–$z$ and $Q$–$z$ curves, representing the soil stiffness in the lateral and axial directions of the piles used in this study. For the monopile length in sand, the calculated nonlinear springs for a single pile were directly incorporated into the FE model, while for the four jacket piles in sand, the pile group effect is considered by incorporating the $p$ and $t$ multipliers into the $p$–$y$ and $t$–$z$ curves, respectively.

Based on the aforementioned soil and pile properties, nonlinear $p$–$y$ and $t$–$z$ curves were defined along the entire lengths of both OWT supporting piles with a spacing of 5 m (shown in Figs. 7(a)–7(f)). As seen in Figs. 7(c) and 7(d), mobilized soil-pile adhesion, $t$, is not influenced by depths beyond 15 m. $Q-z$ curves for both foundation supports are shown in Figs. 7(e) and 7(f). Since their influence only occurs at the pile tips (i.e. 35 m depth), only one curve is used to represent the mobilized pile capacity-axial pile deflection relationship in both cases.

Based on Fig. 7, the nonlinear soil springs were incorporated into respective fixed-base cases of the previously validated OWT models. To validate the use of distributed nonlinear springs in accurately representing the SSI conditions of OWTs, the first natural frequency of the MSOWT–SSI system (nonlinear spring models) obtained in ANSYS was compared to the simplified four spring model (Arany *et al.*[20]) and the simplified three spring model (Schafhirt *et al.*,[30]) as shown in

Table 7. Natural frequencies and modes for JSOWT including different SSI considerations.

| Mode | Description | Frequency with SSI (w/o group effect) (Hz) | Frequency with SSI (with only $p$–$y$ group effect) (Hz) | Difference (%) | Frequency with SSI (with both $p$–$y$ & $t$–$z$ group effects) (Hz) | Difference (%) |
|---|---|---|---|---|---|---|
| 1 | First support structure side-to-side | 0.288 | 0.2874 | 0.06 | 0.2870 | 0.21 |
| 2 | First support structure fore-aft | 0.290 | 0.2890 | 0.38 | 0.2887 | 0.49 |
| 3 | First blade flapwise yaw | 0.515 | 0.5147 | 0.11 | 0.5142 | 0.21 |
| 4 | First blade flapwise pitch | 0.654 | 0.6540 | 0.03 | 0.6539 | 0.05 |
| 5 | First blade collective flapwise | 0.700 | 0.6993 | 0.03 | 0.6992 | 0.05 |
| 6 | First blade edgewise pitch | 0.784 | 0.7833 | 0.14 | 0.7816 | 0.35 |
| 7 | First blade edgewise yaw | 0.866 | 0.8661 | 0.00 | 0.8661 | 0.00 |
| 8 | Second support structure side-to-side | 0.981 | 0.9781 | 0.27 | 0.9775 | 0.33 |
| 9 | Second support structure fore-aft | 1.116 | 1.1147 | 0.12 | 1.1137 | 0.21 |
| 10 | Second blade flapwise yaw | 1.732 | 1.7311 | 0.05 | 1.7309 | 0.06 |
| 11 | Second blade collective flapwise | 2.321 | 2.319 | 0.08 | 2.315 | 0.25 |
| 12 | Second blade flapwise pitch | 1.965 | 1.964 | 0.05 | 1.961 | 0.20 |

*Note*: *w/o: without.

Table 11. The results are 0.173 Hz, 0.175 Hz and 0.170 Hz, respectively. The paper and the latter two models are only 1.15% and 1.7%, thereby validating the SSI model adopted in this study.

To examine the effect(s) of pile group consideration, modal analyzes were conducted on the JSOWT with different SSI considerations, where the first 12 natural frequencies and vibration modes were obtained, as shown in Table 7. It is seen that $p$–$y$ group effect consideration reduced the natural frequencies across all the modes, though by a very little amount, the highest being 0.38% in the first order fore-aft direction. This slight difference is due to the closeness of the $\frac{S}{D}$ value of 5.764 to the marginal value of 6.5. As this marginal value is approached, the effect of group consideration diminishes. Concerning the addition of $t$–$z$ group consideration, very little difference is observed across all the vibration frequencies. In general, the variation in natural frequencies due to group effects consideration reached a maximum difference of 0.49% in only one case. This means that both $p$–$y$ and $t$–$z$ group effects on the vibration frequencies of the JSOWT investigated in this study are negligible and may be ignored during the modal analysis of jacket structures with similar $\frac{S}{D}$ ratio.

Table 8 and Fig. 8 show the comparison results of the natural frequencies of MSOWT and JSOWT including SSI obtained from their modal analyzes. It is observed that the introduction of SSI to the MSOWT causes very significant reductions in the natural frequencies of the tower in both first and second-order vibration modes. This is attributed to the increased flexibility of the monopile inserted into the sea bed, which reduces the stiffness of the tower and the general system. For example, the first natural frequency of the MSOWT in the side-side direction is 0.203 Hz and 0.173 Hz without and with SSI consideration, respectively, which shows a 15% difference. In contrast, SSI inclusion makes an insignificant difference for the blade frequencies. In the case of the JSOWT, SSI inclusion causes a slight reduction to the support frequencies in both first and second-order modes. The first natural frequency

Table 8. Natural frequencies and modes for fixed-base MSOWT and JSOWT including SSI.

| Mode | Description | MSOWT without SSI (Hz) | MSOWT with SSI (Hz) | Difference (%) | JSOWT without SSI (Hz) | JSOWT with SSI (Hz) | Difference (%) |
|---|---|---|---|---|---|---|---|
| 1 | First support structure side-to-side | 0.203 | 0.173 | 15.03 | 0.309 | 0.2870 | 7.08 |
| 2 | First support structure fore-aft | 0.207 | 0.176 | 15.14 | 0.321 | 0.2887 | 10.06 |
| 3 | First blade flapwise yaw | 0.505 | 0.491 | 2.76 | 0.554 | 0.5142 | 7.19 |
| 4 | First blade flapwise pitch | 0.619 | 0.617 | 0.31 | 0.664 | 0.6539 | 1.59 |
| 5 | First blade collective flapwise | 0.725 | 0.714 | 1.54 | 0.720 | 0.6992 | 2.85 |
| 6 | First blade edgewise pitch | 0.846 | 0.774 | 8.50 | 0.864 | 0.7816 | 9.56 |
| 7 | First blade edgewise yaw | 0.893 | 0.857 | 4.01 | 0.880 | 0.8661 | 1.62 |
| 8 | Second support structure side-to-side | 1.481 | 1.326 | 10.43 | 1.168 | 0.9775 | 16.27 |
| 9 | Second support structure fore-aft | 1.524 | 1.366 | 10.39 | 1.241 | 1.1137 | 10.24 |
| 10 | Second blade flapwise yaw | 2.156 | 2.042 | 5.28 | 2.321 | 2.315 | 2.42 |
| 11 | Second blade collective flapwise | 2.490 | 2.350 | 5.62 | 1.965 | 1.9610 | 0.25 |
| 12 | Second blade flapwise pitch | 2.030 | 2.020 | 0.49 | 1.774 | 1.7309 | 0.20 |

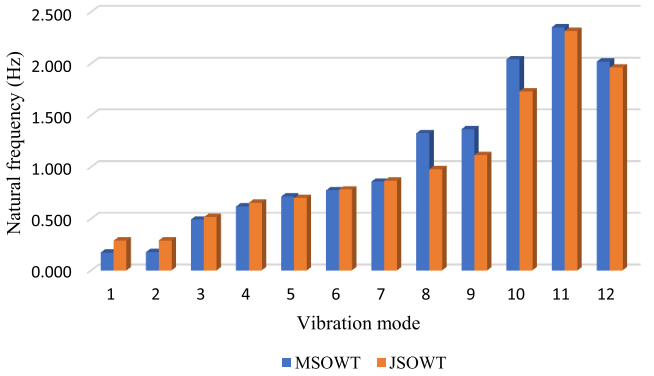


Fig. 8. Comparative vibration frequencies of MSOWT and JSOWT.

of the tower-jacket in the fore-aft direction is 0.321 Hz and 0.2887 Hz without and with SSI consideration, respectively, amounting to a 10% difference. The blade frequencies are also less affected by SSI. In general, SSI has less effect on the natural frequencies of JSOWT than MSOWT, especially with the minimal group pile effect on the former, which in effect makes the four jacket piles behave as though they all act together as a unit while taking full advantage of the lateral stiffness of each pile, in addition to the jacket stiffness and therefore, the higher fundamental natural frequencies recorded. SSI consideration in both types of foundations affects the support vibration modes more than the blade vibration modes. This is because the blades have an indirect connection to the foundations, as against the tower-jacket and tower-monopile, which are in direct contact with the foundations.

Comparing the vibration frequencies of both systems (including SSI consideration), it is observed that the first-order natural frequencies of the JSOWT are generally higher than those of MSOWT; for the blades, the natural frequencies of both structures are largely similar, except for the second-order blade modes. In the second-order vibration modes, however, the support frequencies of the MSOWT are higher than those of the JSOWT. The same trends can be observed in both fixed and flexible conditions.

### 3.4. *Verification of the proposed SSI model*

By using the proposed Eq. (16), the SSI models for MSOWT and JSOWT, i.e. $p$–$y$ curves, were successfully fitted into the two equations shown in Figs. 9(a) and 9(b), respectively. It can be seen that the maximum lateral resistance of soil against soil depth can be perfectly expressed by using only two parameters, with $R^2$ values of 1 in both cases. Further, it is observed that $\propto_2$ remains the same at 0.2344, while $\propto_1$ varied from 1.633 to 0.5666 for MSOWT and JSOWT, respectively. This may suggest that $\propto_1$ is mainly affected by the properties of the (same) soil, while $\propto_2$ is mainly affected by the geometry or other aspects of the foundations.

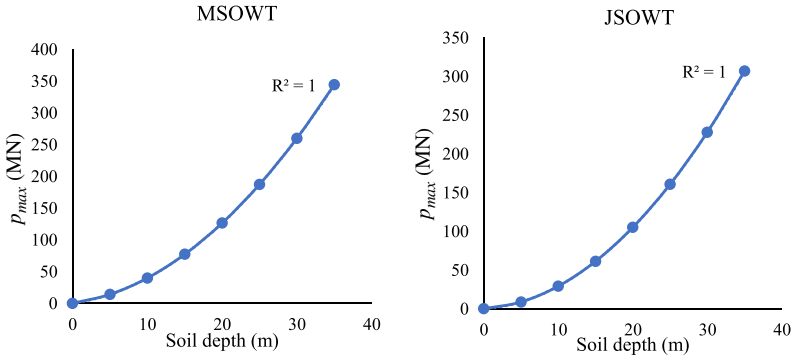


(a) MSOWT (b) JSOWT

Fig. 9. Plots of maximum lateral soil resistance against the depth of soil.

The maximum lateral resistance obtained from the respective $p$–$y$ curves of the two OWT can be used to derive a single soil stiffness at the considered depth, by using Eq. (17). To make the results comparable with the standard method, these stiffness values were obtained across the entire lengths of the piles in steps of 5 m, starting from mudline, to the tip of the piles in both OWT models. For both MSOWT and JSOWT, the respective maximum lateral resistance of soil, maximum lateral displacement, and lateral soil stiffnesses for different depths are computed, as shown in Table 9.

To demonstrate the reliability of this methodology, the lateral soil stiffnesses along the pile lengths obtained for each foundation case was incorporated into the FE models and their modal analyzes were performed. For both OWTs supported on the few parameters SSI models, their first 10 natural frequencies were compared to those of OWTs supported on conventional distributed nonlinear springs, as shown in Table 10. It is observed that the natural frequencies from both SSI models show very close agreements. Maximum differences of 0.71% and 0.66% occur in the first support

Table 9. Properties of the lateral capacity of MSOWT and JSOWT piles/sand.

| Soil depth (m) | Maximum lateral resistance of sand/MSOWT (MN) | Maximum lateral displacement of MSOWT pile(m) | Lateral soil stiffness/ MSOWT (MN/m) | Maximum lateral resistance of sand/ JSOWT (MN) | Maximum lateral displacement of JSOWT pile (m) | Lateral soil stiffness/JSOWT (MN/m) |
|---|---|---|---|---|---|---|
| 5 | 14.024 | 0.05 | 280.476 | 8.692 | 0.05 | 173.844 |
| 10 | 39.766 | 0.10 | 397.656 | 29.1024 | 0.10 | 291.024 |
| 15 | 77.225 | 0.15 | 514.836 | 61.231 | 0.15 | 408.204 |
| 20 | 126.403 | 0.20 | 632.016 | 105.077 | 0.20 | 525.384 |
| 25 | 187.299 | 0.25 | 749.196 | 160.641 | 0.25 | 642.564 |
| 30 | 259.913 | 0.30 | 866.376 | 227.923 | 0.30 | 759.744 |
| 35 | 344.245 | 0.35 | 983.556 | 306.923 | 0.35 | 876.924 |

Table 10. Natural frequencies of MSOWT and JSOWT supported on simplified and discrete $p$–$y$ spring models.

| Mode | Description | MSOWT with distributed nonlinear springs (Hz) | MSOWT with proposed soil springs (Hz) | Difference (%) | JSOWT with $p$–$y$ soil springs (Hz) | JSOWT with proposed soil springs (Hz) | Difference (%) |
|---|---|---|---|---|---|---|---|
| 1 | 1st support structure side-to-side | 0.173 | 0.172 | 0.706 | 0.2870 | 0.2871 | −0.031 |
| 2 | 1st support structure fore-aft | 0.176 | 0.177 | −0.568 | 0.2871 | 0.2890 | −0.658 |
| 3 | 1st blade flapwise yaw | 0.491 | 0.491 | 0.090 | 0.5142 | 0.5145 | −0.058 |
| 4 | 1st blade flapwise pitch | 0.617 | 0.617 | 0.010 | 0.6539 | 0.6540 | −0.014 |
| 5 | 1st blade collective flapwise | 0.714 | 0.713 | 0.043 | 0.6992 | 0.6993 | −0.016 |
| 6 | 1st blade edgewise pitch | 0.774 | 0.775 | −0.004 | 0.7816 | 0.7824 | −0.099 |
| 7 | 1st blade edgewise yaw | 0.857 | 0.856 | 0.128 | 0.8661 | 0.8661 | 0.000 |
| 8 | 2nd support structure side-to-side | 1.326 | 1.321 | 0.354 | 0.9775 | 0.9790 | −0.147 |
| 9 | 2nd support structure fore-aft | 1.366 | 1.363 | 0.220 | 1.1137 | 1.1147 | −0.090 |
| 10 | 2nd blade flapwise yaw | 2.042 | 2.039 | 0.142 | 1.7309 | 1.7316 | –0.040 |

side-side and first support fore-aft directions for MSOWT and JSOWT, respectively. The average difference across the 10 considered modes are only 0.23% and 0.12%, respectively. These minimal differences are attributed to the stiffness contributions of the axial $t$–$z$ and $Q$–$z$ curves in the standard method, which are not included in the proposed methodology. It can also be observed that the proposed methodology gives a closer first natural frequency result to the nonlinear soil spring model than both the simplified three and four-spring models as shown in Table 11.

The derived equations from the proposed few-parameters SSI model contain the entire SSI information while having only two variables. In comparison, seven soil spring parameters are needed using the standard method for SSI in this study. The proposed model largely reduces the number of updating parameters for FE model updating process, while keeping the same accuracy as the standard method. This will reduce computing efforts and time for model updating. Therefore, it has the potential to be applied in future design and analysis of OWTs.

Table 11. Natural frequencies of MSOWT with various SSI models.

| Mode | Description | MSOWT with distributed nonlinear springs (Hz) | MSOWT with Three-soil springs (Hz) | MSOWT with Four-soil springs (Hz) | MSOWT with Proposed SSI model (Hz) |
|---|---|---|---|---|---|
| 1 | 1st support structure side-to-side | 0.173 | 0.170 | 0.175 | 0.172 |

## 4. Conclusion

To examine the implication of cross-deployments of monopile and jacket, this paper conducted a comparative modal analysis of MSOWT and JSOWT deployed in the same sandy deposits using FE models of both structures. Detailed FE models including SSI are developed and analyzed. Fixed and flexible foundation cases of both structures are analyzed. A few-parameters SSI model is also developed in this study for the future application of FE model updating to the identification of support conditions for OWTs. Based on the results of this study, the following conclusions are drawn:

(1) Foundation has a huge influence on the natural frequencies of OWTs they support. For the fixed-base case, JSOWTs generally have higher first-order-support natural frequencies than MSOWTs deployed at same depths. Blade natural frequencies for both structures remain largely unaffected by foundation type, while for the second-order-support modes, the natural frequencies of MSOWTs are larger than those of JSOWTs. Both structures have different mass and stiffness distributions which have huge impacts on their fundamental natural frequencies.
(2) In terms of SSI, monopiles and jackets interact differently with the soil. The flexibility introduced into the system by SSI consideration affects the MSOWTs more than the JSOWTs. This is because the equivalent soil stiffness around the jacket surpasses that around the monopile, leading to the lower fundamental natural frequencies. The group effect for JSOWTs can be ignored if the pile spacing to the diameter ratio is close to the marginal value of 6.5.
(3) A few-parameters SSI model is developed for both MSOWT and JSOWT. These have proven to be very accurate in representing the information contained in the distributed nonlinear SSI model, and thus preserving the fidelity of the FE models in representing their prototypes. In this case, only two parameters are needed to form the $p$–$y$ curve. The number of parameters is less than the simplified methods, such as three or four spring models, while the accuracy is the same as the standard method, with seven parameters (as would be required for the models in this study). Further, the two parameters fitted have the potential to be linked with physical meaning, one related to the soil while the other is related to the foundation. Research efforts can be placed on the further investigation of this model, which has the potential to become a new SSI model for OWTs.

## Acknowledgment

The first author would like to thankfully acknowledge the support of the Petroleum Technology Development Fund (PTDF) under the Federal Government of Nigeria, for sponsoring his PhD studies.

## References


1. Wind Europe, Offshore Wind in Europe: Key trends and statistics 2017, Published February 2018.
2. S. Bhattacharya, Civil engineering aspects of a wind farm and wind turbine structures, in *Wind Energy Engineering* (2017), https://doi.org/10.1016/B978-0-12-809451-8.00012-6.
3. S. Bhattacharya, Challenges in the design of offshore wind turbine foundations, *Eng. Technol. Ref.* (2014).
4. Abdullahi and Y. Wang, Suitability of monopile and jacket foundations for contemporary offshore wind turbines, in *Proc. 15th BGA Young Geotechnical Engineers' Symp.* (2018), pp. 37–38.
5. K. Y. Oh, W. Nam, M. S. Ryu, J. Y. Kim and B. I. Epureanu, A review of foundations of offshore wind energy convertors: Current status and future perspectives, *Renew. Sustain. Energy Rev.* **88**(May) (2018) 16–36, https://doi.org/10.1016/j.rser.2018.02.005.
6. V. Igwemezie, A. Mehmanparast and A. Kolios, Materials selection for XL wind turbine support structures: A corrosion-fatigue perspective, *Marine Struct.* **61** (2018) 381–397.
7. L. V. Andersen, M. J. Vahdatirad, M. T. Sichani and J. D. Sørensen, Natural frequencies of wind turbines on monopile foundations in clayey soils-A probabilistic approach, *Comput. Geotechn.* **43** (2012) 1–11, https://doi.org/10.1016/j.compgeo.2012.01.010.
8. D. Lombardi, S. Bhattacharya and D. Muir Wood, Dynamic soil-structure interaction of monopile supported wind turbines in cohesive soil, *Soil Dyn. Earthquake Eng.* **49** (2013) 165–180, https://doi.org/10.1016/j.soildyn.2013.01.015.
9. S. Bhattacharya and S. Adhikari, Experimental validation of soil-structure interaction of offshore wind turbines, *Soil Dyn. Earthquake Eng.* **31**(5–6) (2011) 805–816, https://doi.org/10.1016/j.soildyn.2011.01.004.
10. S. Jalbi and S. Bhattacharya, Closed-form solution for the first natural frequency of offshore wind turbine jackets supported on multiple foundations incorporating soil-structure interaction, *Soil Dyn. Earthquake Eng.* **113**(June) (2018) 593–613, https://doi.org/10.1016/j.soildyn.2018.06.011.
11. N. Alati, G. Failla and F. Arena, Seismic analysis of offshore wind turbines on bottom-fixed support structures, *Philos. Trans. Royal Soc. A: Math. Phys. Eng. Sci.* **373** (2035) (2015), https://doi.org/10.1098/rsta.2014.0086.
12. S. Bisoi and S. Haldar, Dynamic analysis of offshore wind turbine in clay considering soil-monopile-tower interaction, *Soil Dyn. Earthquake Eng.* **63** (2014) 19–35, https://doi.org/10.1016/j.soildyn.2014.03.006.
13. J. Zhang, W. H. Kang, K. Sun and F. Liu, Reliability-based serviceability limit state design of a jacket substructure for an offshore wind turbine, *Energies* **12**(14) (2019) 2751, https://doi.org/10.3390/en12142751.
14. W. Weijtjens, T. Verbelen, G. De Sitter and C. Devriendt, Foundation structural health monitoring of an offshore wind turbine — a full-scale case study, *Struct. Health Monit.* **15**(4) (2016) 389–402.
15. Y. Xu, G. Nikitas, T. Zhang, Q. Han, S. Bhattacharya and Y. Wang, *Support Condition Monitoring of Offshore Wind Turbines Using Model Updating Techniques* (2019), https://doi.org/10.1177/1475921719875628.
16. S. S. Ahmed and B. Hawlader, Numerical analysis of large-diameter monopiles in dense sand supporting offshore wind turbines. *Int. J. Geomech.* **16**(5) (2016) 1–14, https://doi.org/10.1061/(ASCE)GM.1943-5622.0000633.
17. Z. Guo, L. Yu, L. Wang, S. Bhattacharya, G. Nikitas and Y. Xing, Model tests on the long-term dynamic performance of offshore wind turbines founded on monopiles in sand, *J. Offshore Mech. Arctic Eng.* **137**(4) (2015) 11, https://doi.org/10.1115/1.4030682.

18. Y. Wang, X. Zhu, H. Hao and J. Ou, Spectral element model updating for damage identification using clonal selection algorithm, *Adv. Struct. Eng.* **14**(5) (2011) 837–856.
19. Y. Wang, S. Khoo, A. J. Li and H. Hao, FEM calibrated ARMAX model updating method for time-domain damage identification, *Adv. Struct. Eng.* **16**(1) (2013) 51–60.
20. L. Arany, S. Bhattacharya, J. H. G. Macdonald and S. J. Hogan, Closed-form solution of Eigen frequency of monopile supported offshore wind turbines in deeper waters incorporating stiffness of substructure and SSI, *Soil Dyn. Earthquake Eng.* **83** (2016) 18–32, https://doi.org/10.1016/j.soildyn.2015.12.011.
21. L. Arany, S. Bhattacharya, J. Macdonald and S. J. Hogan, Design of monopiles for offshore wind turbines in 10 steps, *Soil Dyn. Earthquake Eng.* **92** (October 2016) (2017) 126–152, https://doi.org/10.1016/j.soildyn.2016.09.024.
22. A. H. Augustesen, K. T. Brødbæk, M. Møller, S. P. H. Sørensen, L. B. Ibsen, T. S. Pedersen and L. Andersen, Numerical modelling of large-diameter steel piles at Horns Rev, in *Proc. TwelfthInt. Conf. Civil, Structural and Environmental Engineering Computing*, Vol. 515, 2009.
23. J. Jonkman, S. Butterfield, W. Musial and G. Scott, *Definition of a 5-MW Reference Wind Turbine for Offshore System Development*, Technical Report, United States (February) (2009), https://doi.org/10.2172/947422.
24. H. Zuo, K. Bi and H. Hao, Dynamic analyses of operating offshore wind turbines including soil-structure interaction, *Eng. Struct.* **157** (November 2017) (2018) 42–62, https://doi.org/10.1016/j.engstruct.2017.12.001.
25. F. Vorpahl and D. Kaufer, *Technical Report Description of a Basic Model of the 'UpWind Reference Jacket' for Code Comparison in the OC4 Project Under IEA Wind Annex 30* (2013).
26. H. Zuo, K. Bi and H. Hao, Mitigation of tower and out-of-plane blade vibrations of offshore monopile wind turbines by using multiple tuned mass dampers, *Struct. Infrastruct. Eng.* **15**(2) (2019) 269–284, https://doi.org/10.1080/15732479.2018.1550096.
27. S. Jalbi, M. Shadlou and S. Bhattacharya, Practical method to estimate foundation stiffness for design of offshore wind turbines, in *Wind Energy Engineering: A Handbook for Onshore and Offshore Wind Turbines* (Elseiver, 2017), pp. 329–352, https://doi.org/10.1016/B978-0-12-809451-8.00016-3.
28. V. del Campo, D. Ragni, D. Micallef, J. Diez and C. J. Simão Ferreira, Estimation of loads on a horizontal axis wind turbine, *Wind Energy* **18**(11) (2015) 1875–1891, https://doi.org/10.1002/we.
29. M. Harte, B. Basu and S. R. Nielsen, Dynamic analysis of wind turbines including soil-structure interaction, *Eng. Struct.* **45** (2012) 509–518.
30. S. Schafhirt, A. Page, G. R. Eiksund and M. Muskulus, Influence of soil parameters on the fatigue lifetime of offshore wind turbines with monopile support structure, *Energy Procedia* **94**(January) (2016) 347–356, https://doi.org/10.1016/j.egypro.2016.09.194.
31. B. Huang, R. J. Bathurst and K. Hatami, Numerical study of reinforced soil segmental walls using three different constitutive soil models, *J. Geotechn. Geoenviron. Eng.* **135** (10) (2009) 1486–1498.
32. F. J. Zwerneman and K. A. Digre, 22nd edition of API RP 2A recommended practice for planning, designing and constructing fixed offshore platforms — Working stress design, *Proc. Annual Offshore Technology Conf.* 3(December 2000) (2010) 2364–2372.
33. W. Shi, H. C. Park, C. W. Chung, H. K. Shin, S. H. Kim, S. S. Lee and C. W. Kim, Soil-structure interaction on the response of jacket-type offshore wind turbine, *Int. J.*

*Precision Eng. Manufacturing — Green Technol.* **2**(2) (2015) 139–148, https://doi.org/10.1007/s40684-015-0018-7.
34. S. Schafhirt, A. Page, G. R. Eiksund and M. Muskulus, Influence of soil parameters on the fatigue lifetime of offshore wind turbines with monopile support structure, *Energy Procedia* **94**(January) (2016) 347–356, https://doi.org/10.1016/j.egypro.2016.09.194.
35. M. Sajjad Fayyazi, M. Taiebat and W. D. Liam Finn, Group reduction factors for analysis of laterally loaded pile groups, *Canadian Geotechn. J.* **51**(7) (2014) 758–769, https://doi.org/10.1139/cgj-2013-0202.
36. K. M. Rollins and R. J. Olsen, Pile spacing effects on lateral pile group behaviour, *J. Geotechn. Geoenviron. Eng.* **132**(10) (2006) 1272–1283, https://doi.org/10.1017/CBO9781107415324.004.
37. D. A. Brown, C. Morrison and L. C. Reese, Lateral load behaviour of pile group in sand, *J. Geotechn. Eng.* **114**(11) (1988) 1261–1276.
38. R. D. Chellis, Pile foundations, in *ch. 7 in Foundations Engineering*, ed. G. A. Leonards (McGraw-Hill, New York, 1962).
39. H. G. Poulos and E. H. Davis, *Pile Foundation Analysis and Design* (JohnWiley & Sons, Ltd, Chichester, 1980).
40. A. Kezdi, The bearing capacity of piles and pile groups. in *Proc. 4th Int. Conf. S. M. & F. E.*, Vol. 2 (Springer, 1957), pp. 46–51.
41. H. Cambefort, La Force Portante des Groupes de Pieux, in *Proc. 3rd Int. Conf. S. M. & F. E.*, Vol. 2 (Springer, 1953), pp. 22–29.
42. Y. Wang and T. Zhang, Finite element model updating using estimation of distribution algorithm, in *SHMII-6 2013: Proc. 6th Int. Conf. Structural Health Monitoring of Intelligent Infrastructure* (Hong Kong Polytechnic University, 2013), pp. 1–8.
43. J. D. Allen, L. C. Reese. Small scale tests for the determination of py curves in layered soils, *Offshore Technology Conference*, 5–8 May 1980, Houston, Texas.